

Interlayer confinement mediated oxidation of Americium by sodium bismuthate and stability of its higher redox states in acidic solution

Parveen K. Verma, Arunasis Bhattacharyya*, Prasanta K. Mohapatra *

Radiochemistry Division, Bhabha Atomic Research Centre,
Mumbai, Maharashtra, INDIA

Contents

NaBiO ₃ characterization	2
X-ray diffraction analysis.....	2
ATR-FTIR of NaBiO ₃ .xH ₂ O (x= 2-3)and its derivatives	3
Hexavalent Americium reduction rate.....	4
Am ³⁺ oxidation at higher ionic strength	5
Americium oxidation assisted dissolution of NaBiO ₃ .xH ₂ O (x= 2-3).....	7
References.....	9

List of Table and Figures

Table S1: Common methods for oxidizing Am ³⁺ to AmO ₂ ²⁺ in acidic medium.....	3
Figure S 1. The ATR-FTIR of pristine, acid treated (H ⁺ -form), and Eu ³⁺ sorbed NaBiO ₃ .xH ₂ O (x= 2-3) at different time of equilibration.....	4
Figure S 2. Variation in the rate of AmO ₂ ²⁺ conversion to the lower valent Am oxidation state.....	5
Figure S3. Comparison of XRD spectra of pristine NaBiO ₃ , with acid equilibrated NaBiO ₃ at different time intervals in pH 1 HNO ₃	6
Figure S 4. The vis-NIR spectra of initial Am ³⁺ and after its oxidation in presence and absence of 1 M NaClO ₄ in pH 1 HNO ₃	6
Figure S 5. The emission and excitation spectra Eu ³⁺ of aqueous phase before and after equilibration with NaBiO ₃ .xH ₂ O (x= 2-3).	7
Figure S 6. The vis-NIR spectra of Am-NaBiO ₃ .xH ₂ O (x= 2-3) supernatant after 20 minutes of equilibration at pH 1 HNO ₃	8

Table S1: Common methods for oxidizing Am^{3+} to AmO_2^{2+} in acidic medium.

Initial	Conditions	Final	Ref.
Am^{3+}	NaBiO_3 at room temperature in nitric acid	AmO_2^{2+}	1, 2
	NaBiO_3 at room temperature in H_3PO_4		3
	Cu^{3+} -iodate in nitric acid		4
	Excess $(\text{NH}_4)_2\text{S}_2\text{O}_8$ in 0.1 M nitric acid at 85°C		5
	$\text{Na}_4\text{XeO}_6/\text{Ag}^+$ in 1 M nitric acid		6
	0.013 M $\text{CsSO}_4\text{F}/0.001$ M Ag^+ in 0.9 M nitric acid		7
	0.5% AgNO_3 / 2.5% $(\text{NH}_4)_2\text{S}_2\text{O}_8$ in 0.3 M nitric acid		8
	Electrochemical in 6 M HClO_4		5
	Electrochemical oxidation using a dipyrazinylpyridine modified ITO electrode in 0.1 M nitric acid		9
	Photolytic conversion in 0.1 M nitric acid using a $\text{Ti} \text{TiO}_2$ electrode		10
	Resonance enhanced multi photon excitation for Am^{3+} oxidation		11

NaBiO_3 characterization

X-ray diffraction analysis

The XRD data of the NaBiO_3 used in the present study matched well with the JCPDF file number PDF # 30-1161, suggesting the presence of hydrated form of NaBiO_3 as $\text{NaBiO}_3 \cdot x\text{H}_2\text{O}$ ($x=2-3$)(NBO).¹² The previous literature studies on the Am^{3+} oxidation by NaBiO_3 is mainly done in HNO_3 medium, except that by Rice et al.,³ where other acidic mediums were chosen. Therefore, it is essential to understand the structural changes in NaBiO_3 upon contact with HNO_3 . The previous study¹³ in this direction showed color change of pristine NaBiO_3 to dark brown upon contact with HNO_3 . The study used different HNO_3 : NaBiO_3 molar ratios and the mixture was equilibrated for 2 hours and the structural changes were followed by XRD. Since the overall composition, purity, nature of impurity in sodium bismuthate, can vary from source to source and can have profound effect on its properties; we have revisited the effect of HNO_3 on

NaBiO_3 at a lower acidity (pH 1) suitable for the present studies. The $\text{NaBiO}_3 \cdot x\text{H}_2\text{O}$ ($x = 2-3$) was equilibrated with pH 1 HNO_3 for 24 hours and the solid was collected after centrifugation, air dried followed by which the XRD was recorded. The color of $\text{NaBiO}_3 \cdot x\text{H}_2\text{O}$ ($x = 2-3$) changed from light yellow to brown (Fig. 1(a)) in <30 minutes of equilibration with pH1 HNO_3 which was also observed by others.¹³ The XRD of the acid equilibrated $\text{NaBiO}_3 \cdot x\text{H}_2\text{O}$ ($x = 2-3$) (H^+ -form) suggested loss of crystallinity and formation of a different amorphous phase than $\text{NaBiO}_3 \cdot x\text{H}_2\text{O}$ ($x = 2-3$) (Fig. 1(a)) as also observed by Kozma et al.¹³

ATR-FTIR of $\text{NaBiO}_3 \cdot x\text{H}_2\text{O}$ ($x = 2-3$) and its derivatives

The FTIR spectra showed change in the 1000-2000 cm^{-1} region for the acid treated $\text{NaBiO}_3 \cdot x\text{H}_2\text{O}$ ($x = 2-3$) as compared with the pristine compound (Fig. S1). The ATR-FTIR of the $\text{NaBiO}_3 \cdot x\text{H}_2\text{O}$ ($x = 2-3$) and acid treated $\text{NaBiO}_3 \cdot x\text{H}_2\text{O}$ ($x = 2-3$) shows substantial difference. The peak in the 500-1000 cm^{-1} region due to the Bi-O-Bi stretching¹⁴ is shifted from 846 cm^{-1} to 820 cm^{-1} suggesting structural changes in the BiO_6 octahedra of $\text{NaBiO}_3 \cdot x\text{H}_2\text{O}$ ($x = 2-3$). The Bi-O stretching peak at 1390 cm^{-1} also shifted to 1378 cm^{-1} , with a new peak at 1328 cm^{-1} . These changes can be attributed due to the in situ conversion of $\text{Bi}^{5+} \rightarrow \text{Bi}^{3+}$ in the BiO_6 octahedra of $\text{NaBiO}_3 \cdot x\text{H}_2\text{O}$ ($x = 2-3$).^{13, 15} Strong absorption peaks in the range of 1600–1700 cm^{-1} and 3000–3800 cm^{-1} are characteristic absorptions of water¹⁶, along with some BiO_3^- absorption peaks. Although, the exact assignment of the BiO_3^- and water in 1600–1700 cm^{-1} region is difficult but the change in the water structure after acid treatment can be pointed out by change in the >3000 cm^{-1} region.

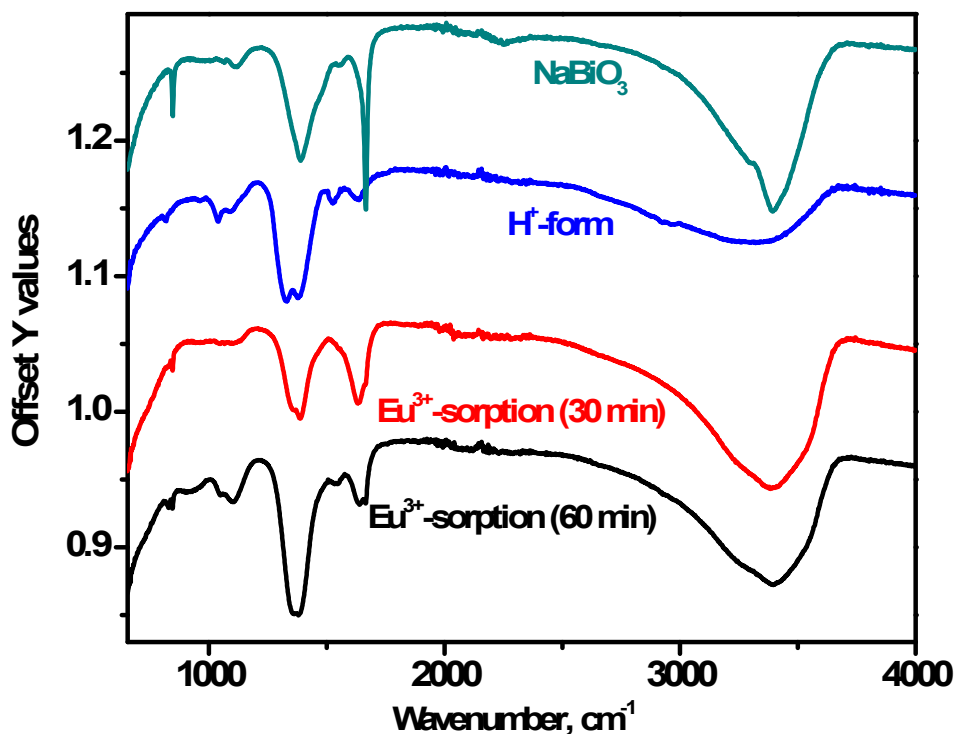


Figure S 1. The ATR-FTIR of pristine, acid treated (H⁺-form), and Eu³⁺ sorbed NaBiO₃.xH₂O (x= 2-3) at different time of equilibration.

The FTIR of Eu³⁺ sorbed NaBiO₃.xH₂O (x= 2-3) at two different equilibration time (30 minutes and 60 minutes) was also recorded. The two FTIR spectra are mainly dominated by the features corresponding to the H⁺-form of the NaBiO₃.xH₂O (x= 2-3), especially when equilibrated for longer time interval. The ATR-FTIR after 30 minutes of equilibration shows features due to both NaBiO₃.xH₂O (x= 2-3) and H⁺-form due to its incomplete conversion to H⁺-form.

Hexavalent Americium reduction rate

The reduction of AmO₂²⁺ after equilibration with NaBiO₃.xH₂O (x= 2-3) at pH 1 HNO₃ was followed with time at different temperature. All the equilibration for oxidation was carried out at 25 °C and the sample was transferred in 1 ml screw cap quartz cuvette with 10 mm path length for temperature and time dependent spectral measurements. The temperature dependent reduction of AmO₂²⁺ was followed using coupled Peltier attachment of Jasco V-530 double beam spectrophotometer. We didn't observe any definite trends for the AmO₂²⁺ decay with temperature and the rates of the decay also varies just by changing the centrifugation speed for

separation of solid $\text{NaBiO}_3 \cdot x\text{H}_2\text{O}$ ($x= 2-3$) from suspension. The reasoning for this variation along with other observation is discussed in main manuscript.

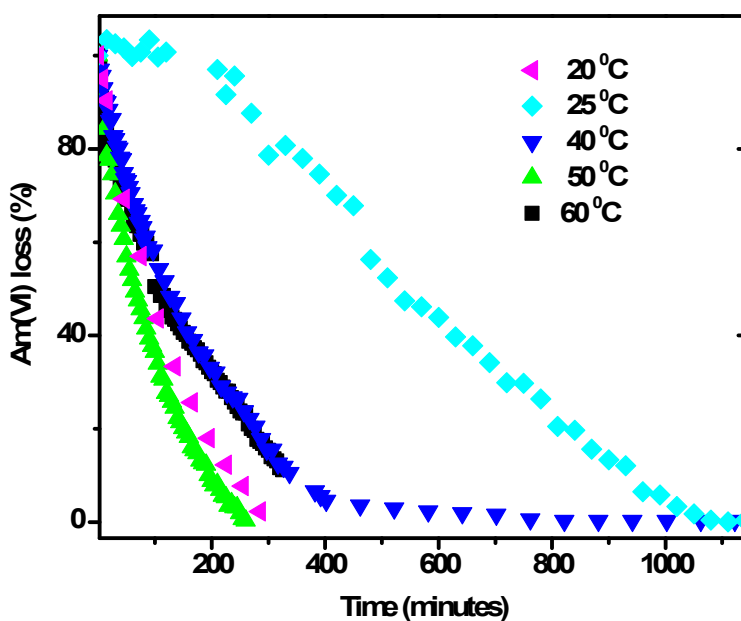


Figure S 2. Variation in the rate of AmO_2^{2+} conversion to the lower valent Am oxidation state.

DLS studies

The DLS studies were performed to understand the effect of colloidal particle density on the Am^{3+} oxidation and its stability of its higher oxidation states. The NaBiO_3 was equilibrated with pH 1 for 15-20 minutes and centrifuged at 500RCF and 3000 RCF for different time. The particle size distribution in the supernatant was followed using Particle size analyzer (Corduan, France). The 30 nm standard (NanosphereTM size standard (Thermo fisher)) was used prior to the supernatant measurements to check the machine performance. The standard shows a value of 31.0 (± 0.2) nm using inbuilt cumulant algorithm for the auto correlation function (ACF) fitting. The decay of ACF for sample centrifuged at 500 RCF for 5 minute and 10 minutes confirms the presence of NaBiO_3 particle in the supernatant. However, supernatant obtained after 3000 RCF centrifugation for 10 minutes shows poor ACF decay and the cumulant analysis fails to give any suitable size (**Fig. S3**). This poor ACF decay suggests absence of any particle in the supernatant.

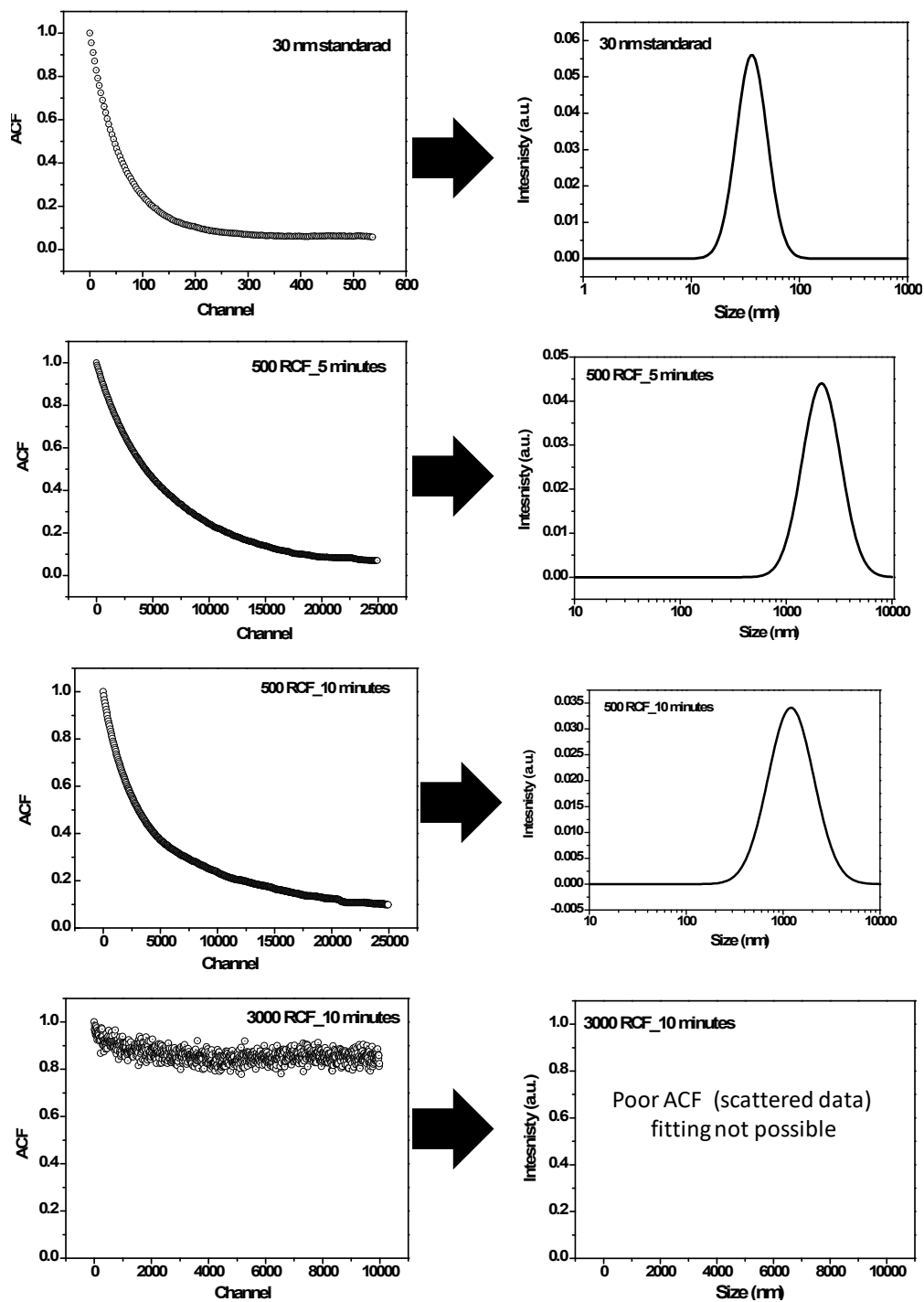


Figure S3. The variation in the autocorrelation function (ACF) after centrifugation at 500 RCF for 5 and 10 minutes and 3000 RCF for 10 minutes for NaBiO₃ suspension equilibrated with pH 1 HNO₃ (left). The resultant size distribution using cumulant algorithm under different centrifugation conditions (right).

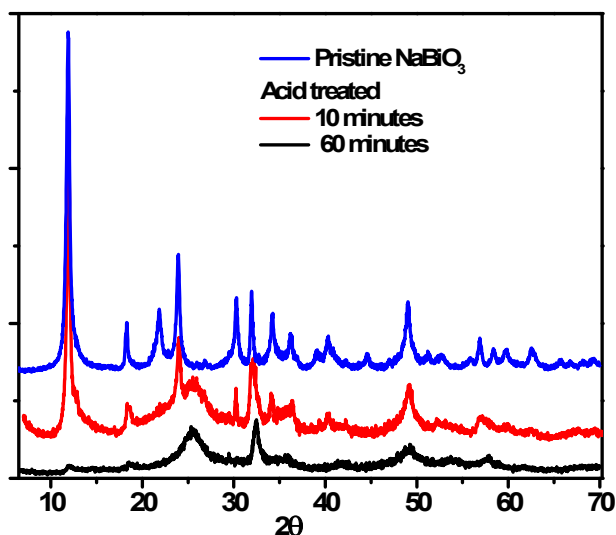


Figure S4. Comparison of XRD spectra of pristine NaBiO₃, with acid equilibrated NaBiO₃ at different time intervals in pH 1 HNO₃.

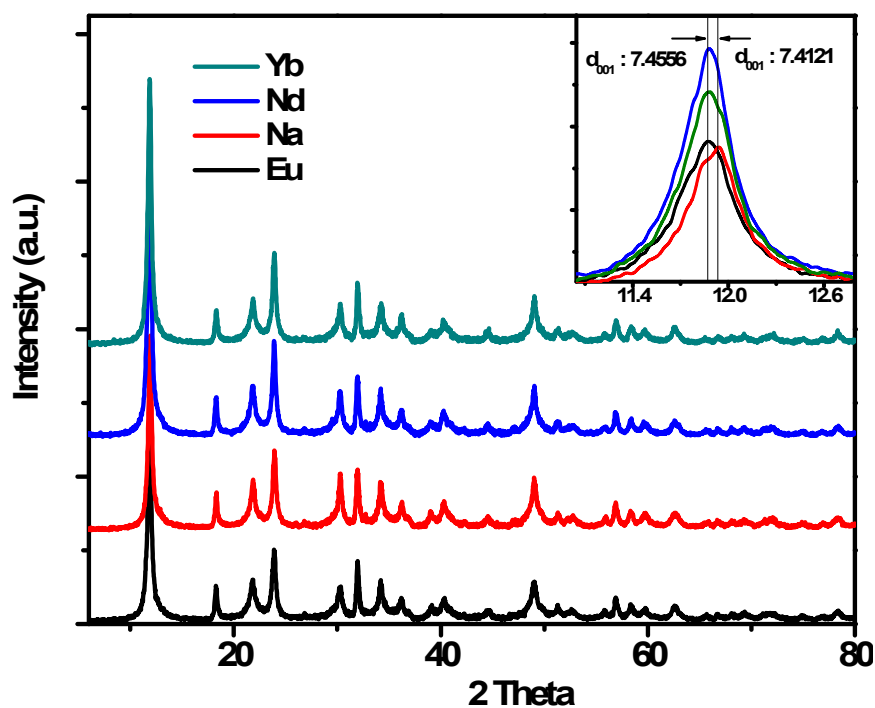


Figure S5. The XRD of the pristine NaBiO₃ and lanthanides loaded NaBiO₃, pH ~4, Time of equilibration: 24 hrs, [Ln]: 0.1 M, NaBiO₃ : 30 mg/ml.

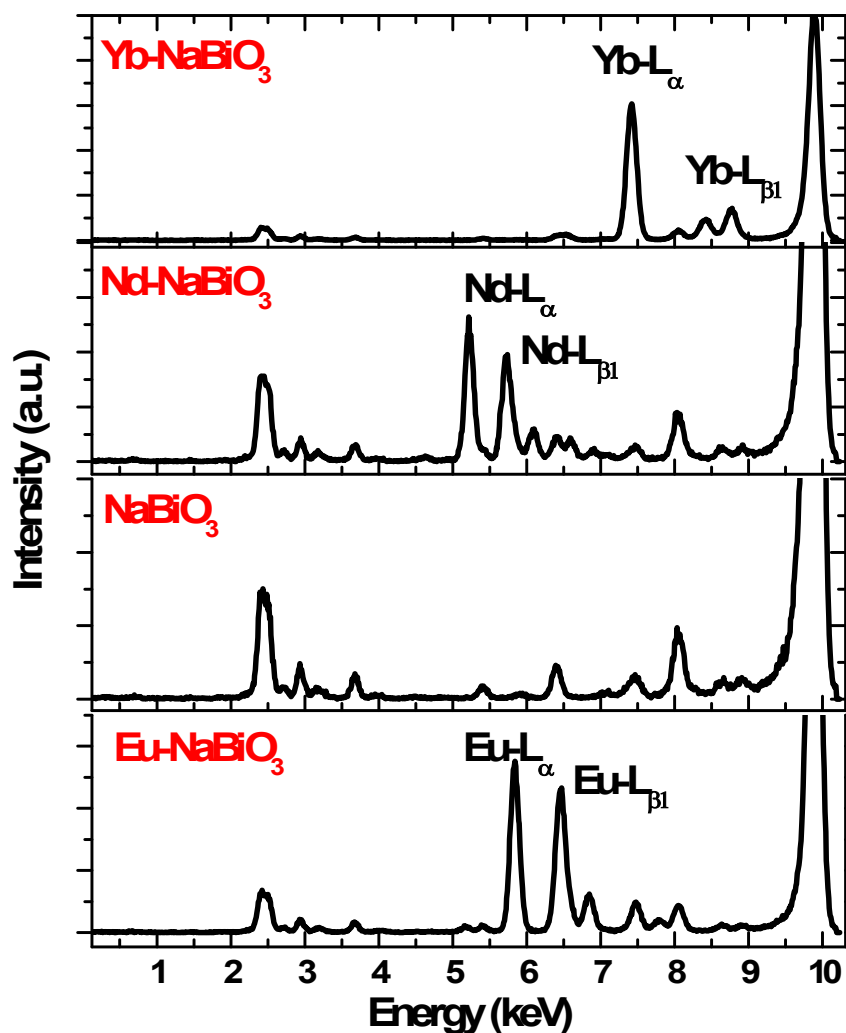


Figure S6. The XRF of the pristine NaBiO_3 and lanthanides loaded NaBiO_3 , pH ~ 4 , Time of equilibration: 24 hrs, $[\text{Ln}]$: 0.1 M, NaBiO_3 : 30 mg/ml.

Am^{3+} oxidation at higher ionic strength

The oxidation of Am^{3+} at higher ionic strength (1M NaClO_4) was carried out at pH 1 HNO_3 and the results were compared to the Am^{3+} oxidation without any NaClO_4 . The quantitative oxidation of Am^{3+} (>95 %) was observed in the absence of NaClO_4 within 20 minutes whereas only 80-83% oxidation of Am^{3+} was observed at higher ionic strength even after 120 minutes of equilibration with $\text{NaBiO}_3 \cdot x\text{H}_2\text{O}$ ($x = 2-3$) in pH 1 HNO_3 .

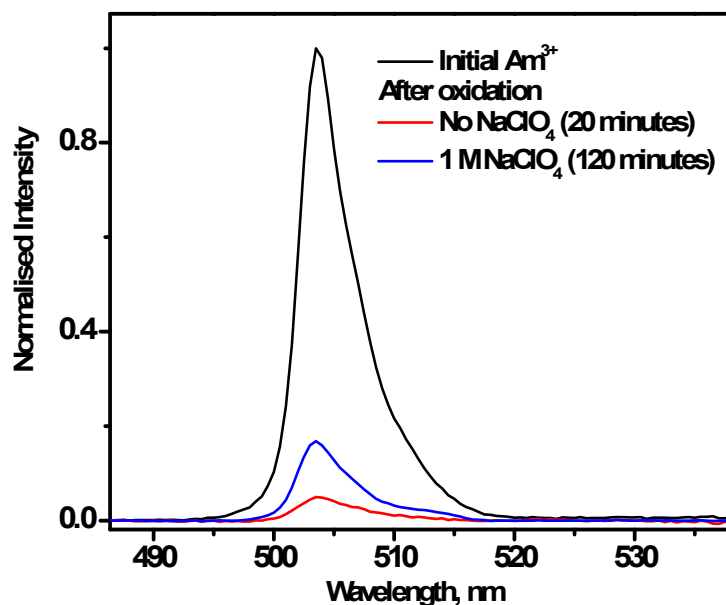


Figure S 7. The vis-NIR spectra of initial Am^{3+} and after its oxidation in presence and absence of 1 M NaClO_4 in pH 1 HNO_3

Americium oxidation assisted dissolution of $\text{NaBiO}_3 \cdot x\text{H}_2\text{O}$ ($x=2-3$)

The dissolution of $\text{NaBiO}_3 \cdot x\text{H}_2\text{O}$ ($x=2-3$) was investigated in the presence of redox inactive Eu^{3+} and redox active Am^{3+} in pH 1 HNO_3 . The photoluminescence of the Eu^{3+} aqueous solution before and after equilibration with $\text{NaBiO}_3 \cdot x\text{H}_2\text{O}$ ($x=2-3$) studies suggested >99% uptake of Eu^{3+} onto the $\text{NaBiO}_3 \cdot x\text{H}_2\text{O}$ ($x=2-3$) (Fig. S4). The Uv-vis spectra of the supernatant of Eu^{3+} - $\text{NaBiO}_3 \cdot x\text{H}_2\text{O}$ ($x=2-3$) system lacks any peak of BiO_3^- even after 72 hrs of equilibration. However, distinct peak for BiO_3^- (Fig. S4, yellow region,) along with peak at 503 due to residual Am^{3+} (grey region, Fig. S5) was seen for Am^{3+} - $\text{NaBiO}_3 \cdot x\text{H}_2\text{O}$ ($x=2-3$) system. The lack of peak in the Eu^{3+} - $\text{NaBiO}_3 \cdot x\text{H}_2\text{O}$ ($x=2-3$) system and its presence in Am^{3+} - $\text{NaBiO}_3 \cdot x\text{H}_2\text{O}$ ($x=2-3$) system, suggest role of Am^{3+} redox transformation in the dissolution of $\text{NaBiO}_3 \cdot x\text{H}_2\text{O}$ ($x=2-3$) even at pH 1 HNO_3 . This observation along with Ce^{3+} oxidation and discussed in the main manuscript.

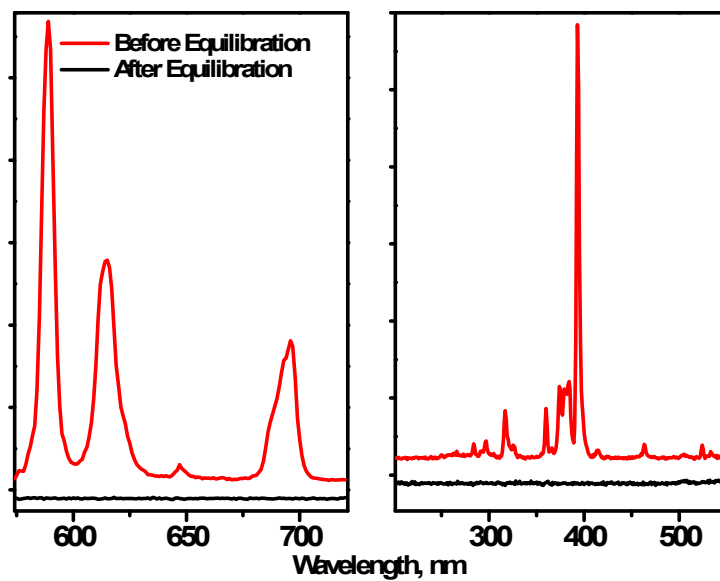


Figure S8. The emission and excitation spectra Eu^{3+} of aqueous phase before and after equilibration with $\text{NaBiO}_3 \cdot x\text{H}_2\text{O}$ ($x=2-3$).

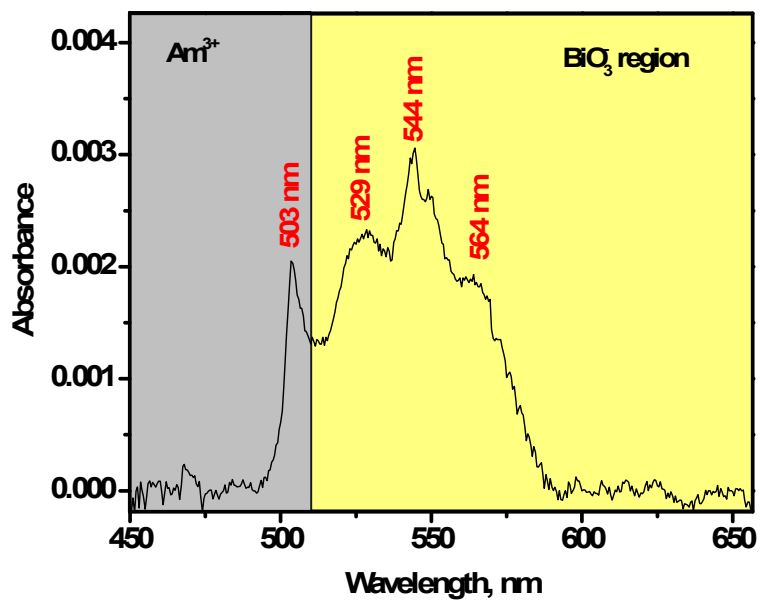


Figure S 9. The vis-NIR spectra of Am-NaBiO₃.xH₂O (x= 2-3) supernatant after 20 minutes of equilibration at pH 1 HNO₃

1. M. Hara and S. Suzuki, *Journal of Radioanalytical Chemistry*, 1977, **36**, 95-104.
2. B. J. Mincher, L. R. Martin and N. C. Schmitt, *Inorg. Chem.*, 2008, **47**, 6984-6989.
3. N. T. Rice, E. Dalodière, S. L. Adelman, Z. R. Jones, S. A. Kozimor, V. Mocko, H. D. Root and B. W. Stein, *Inorg. Chem.*, 2022, **61**, 12948-12953.
4. S. I. Sinkov and G. J. Lumetta, *Radiochimica Acta*, 2015, **103**, 541-552.
5. L. B. Asprey, S. E. Stephanou and R. A. Penneman, *J. Am. Chem. Soc.*, 1951, **73**, 5715-5717.
6. H. P. Holcomb, *Anal. Chem.*, 1965, **37**, 415-415.
7. E. Appebnan, H. Diamond, E. Horwitz and J. Sullivan, *Radiochimica Acta*, 1991, **55**, 61-64.
8. B. Myasoedov, V. Mikhailov, I. Lebedev, O. Koiro and V. Y. Frenkel, *Preparation and stability of Am (IV) and Am (VI) in phosphoric acid solutions*, Inst. of Geochemistry and Analytical Chemistry, Moscow, 1973.
9. M. J. Lopez, M. V. Sheridan, J. R. McLachlan, T. S. Grimes and C. J. Dares, *Chem. Commun.*, 2019, **55**, 4035-4038.
10. M. V. Sheridan, J. R. Gonzalez-Moya, J. R. McLachlan, T. S. Grimes and C. J. Dares, *ACS Applied Energy Materials*, 2021, **4**, 11854-11857.
11. S. Matsuda, K. Yokoyama, T. Yaita, T. Kobayashi, Y. Kaneta, M. Simonnet, T. Sekiguchi, M. Honda, K. Shimojo, R. Doi and N. Nakashima, *Science Advances*, 2022, **8**, 1991-1991.
12. Y. Feng, X. Huang, Q. Zhan and D. Jiang, *Journal of Materials Science: Materials in Electronics*, 2019, **30**, 10543-10549.
13. K. Kozma, T. W. Surta, P. I. Molina, I. Lyubinetsky, W. Stoxen, N. M. Byrne, M. Dolgos and M. Nyman, *J. Solid State Chem.*, 2018, **263**, 216-223.
14. L. Liu, J. Jiang, S. Jin, Z. Xia and M. Tang, *CrystEngComm*, 2011, **13**, 2529-2532.
15. Y. Ding, F. Yang, L. Zhu, N. Wang and H. Tang, *Applied Catalysis B: Environmental*, 2015, **164**, 151-158.
16. F. Gan, K. Wu, F. Ma and C. Du, *Journal*, 2020, **25**.

References